

Iterative Thresholding Methods for Longest Minimal Length Partitions

Shilong Hu^a, Hao Liu^b, Dong Wang^{a,c}

^a*School of Science and Engineering, The Chinese University of Hong Kong, Shenzhen, Guangdong 518172, China*

^b*Department of Mathematics, Hong Kong Baptist University, Kowloon Tong, Hong Kong*

^c*Shenzhen International Center for Industrial and Applied Mathematics, Shenzhen Research Institute of Big Data, Guangdong 518172, China*

Abstract

In this paper, we introduce two iterative methods for longest minimal length partition problem, which asks whether the disc (ball) is the set maximizing the total perimeter of the shortest partition that divides the total region into sub-regions with given volume proportions, under a volume constraint. The objective functional is approximated by a short-time heat flow using indicator functions of regions and Gaussian convolution. The problem is then represented as a constrained max-min optimization problem. Auction dynamics is used to find the shortest partition in a fixed region, and threshold dynamics is used to update the region. Numerical experiments in two-dimensional and three-dimensional cases are shown with different numbers of partitions, unequal volume proportions, and different initial shapes. The results of both methods are consistent with the conjecture that the disc in two dimensions and the ball in three dimensions are the solution of the longest minimal length partition problem.

Keywords: threshold dynamics, auction dynamics, fencing problem, longest minimal length partitions, volume constrained partitions

2000 MSC: 49M20, 49Q05, 49M05, 41A30

1. Introduction

The fencing problem has a long history and is rooted in the division of land using fences. One of the earliest studies in this field can be traced back to [1], which investigated the scenario of a cylinder floating in water. This problem was further explored in subsequent studies such as [2, 3, 4], in which one considers dividing a convex set into two equal-area sets and studies the optimal arc length of the fence.

In the 1950s, Pólya raised a question in [5]: Among all convex sets in \mathbb{R}^2 with a fixed area, which one has the longest shortest arc that bisects the area? This question remained unresolved throughout the last century. According to [6], Santaló made a conjecture that the disc is the answer. Until 2012, the conjecture was proven in [7]. A similar conjecture in high dimensions was proposed in [8] and [9] after Pólya. It considers the case of dividing a region in \mathbb{R}^d space into two sub-regions of arbitrary given volume proportions, and asks whether the least length of arc to divide a ball is greater than the least length of arc to divide any other convex body of the same volume. The new conjecture generalizes the bisection problem to arbitrary volume constraints. In the literature, some analytical results have been presented in [10] and [11], which offer partial proofs for this

Email addresses: shilonghu@link.cuhk.edu.cn (Shilong Hu), haoliu@hkbu.edu.hk (Hao Liu), wangdong@cuhk.edu.cn (Dong Wang)

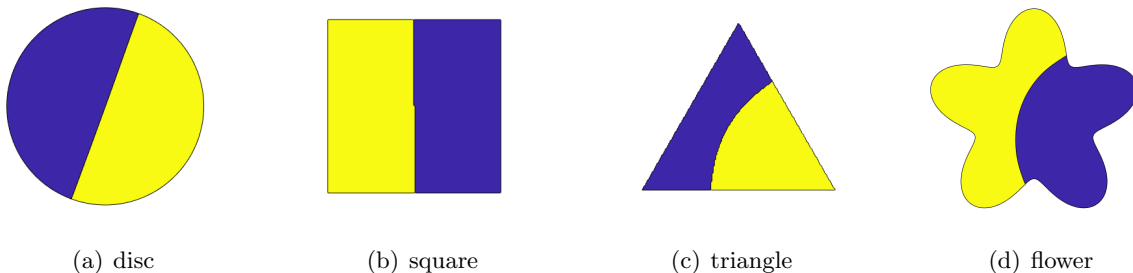


Figure 1: The shortest partitions of different Ω in Pólya's question. The partitions are computed numerically by auction dynamics in Section 3.

conjecture. As of now, the conjecture remains unanswered for the case of three-dimensional space and for large fraction areas in the two-dimensional case (except for bisection).

In [12], the authors extend the conjecture even further. They investigate whether the disc in two dimensions and the ball in three dimensions still provide the longest minimal length partitions when the region is divided into more than two parts. The mathematical description of it is given below.

Given $\Omega \subset \mathbb{R}^d$ as an open, connected region with Lipschitz boundary and the number of partition $n > 1$, $(\omega_1, \dots, \omega_n)$ is said to be a partition of Ω if $\bigcup_{i=1}^n \omega_i = \Omega$ and $\omega_i \cap \omega_j = \emptyset$ for any $1 \leq i < j \leq n$. Given a vector $\mathbf{c} = (c_1, \dots, c_n) \in \mathbb{R}^n$ with $c_i > 0$ and $\sum_{i=1}^n c_i = 1$, the shortest partition of Ω with volume constraint \mathbf{c} is defined by

$$SP(\Omega, \mathbf{c}) = \arg \min_{(\omega_i)_{i=1}^n} \left\{ \sum_{i=1}^n \text{Per}_\Omega(\omega_i) : (\omega_i)_{i=1}^n \text{ is a partition of } \Omega, |\omega_i| = c_i |\Omega| \right\},$$

where $|\cdot|$ is the Lebesgue measure, and $\text{Per}_\Omega(\omega_i)$ is the relative perimeter of ω_i on Ω . The relative isoperimetric profile of the partition is defined as

$$PI(\Omega, \mathbf{c}) = \min_{(\omega_i)_{i=1}^n} \left\{ \sum_{i=1}^n \text{Per}_\Omega(\omega_i) : (\omega_i)_{i=1}^n \text{ is a partition of } \Omega, |\omega_i| = c_i |\Omega| \right\}.$$

Then the longest minimal length partitions problem is formulated by

$$\max_{|\Omega|=V} PI(\Omega, \mathbf{c}). \quad (1)$$

When $n = 2$, problem (1) degenerates into the original fencing problem. If we further set the dimension $d = 2$ and $\mathbf{c} = (0.5, 0.5)$, the problem is exactly the same one as Pólya raised.

The relative perimeter here is defined by using the total variation. Suppose χ_ω is the indicator function of ω , then

$$\text{Per}_\Omega(\omega) = TV(\chi_\omega, \Omega),$$

where

$$TV(u, \Omega) = \sup \left\{ \int_\Omega u \text{div} g : g \in C_c(\Omega, \mathbb{R}^d), \|g\|_\infty \leq 1 \right\}$$

is the total variation of u on Ω , and $C_c(\Omega, \mathbb{R}^d)$ means the space of C^∞ vector-valued functions on Ω with compact support. Intuitively speaking, $\text{Per}_\Omega(\omega) = |\partial\omega \setminus \partial\Omega|$, and $\sum_{i=1}^n \text{Per}_\Omega(\omega_i)$ in $PI(\Omega, \mathbf{c})$ is $\frac{1}{2}(\sum_{i=1}^n |\partial\omega_i| - |\partial\Omega|)$. More details about the relative perimeter can be found in [13].

In [12], the authors propose a phase-field method based on shape derivatives to numerically simulate the longest minimal length partitions. The method involves using a Modica-Mortola approximation to represent the perimeter, and the total region is parameterized using a radial function discretized with Fourier coefficients. The authors update the total region by iteratively modifying the Fourier coefficients based on shape derivatives. To maintain the volume constraint, they project the Fourier coefficients using a homothety at each iteration step. The authors claim that the results of their method provide numerical evidence for the conjecture that for any fixed \mathbf{c} , the disk is always the maximizer in two dimensions, and the ball is always the maximizer in three dimensions.

In [14] the authors present a short-time heat flow approximation for the boundary integral energy of functions with bounded variation. This approximation utilizes indicator functions and Gaussian convolution and does not require taking derivatives of the functions. In [15, 16, 17], Merriman, Bence, and Osher (MBO) developed a threshold dynamics method for interface motion. The method has been proved to converge to mean curvature flow in [18, 19]. Esedoglu and Otto further extended this method to the multi-phase case in [20]. The method can be applied to general multiphase problems with arbitrary surface tensions. The MBO method and its idea have gained recognition for simplicity and stability, and have been widely applied in various areas such as motion by mean curvature for filaments [21], volume-preserving interface motion [22, 23], image processing [24, 25, 26, 27, 28], graph data processing [29, 30, 31], foam bubbles [32], grain boundary motion [33] and wetting phenomena on solid surfaces [34]. Recently, connections among the MBO method, operator-splitting methods and deep neural networks are pointed out in [35, 36, 37].

Numerous algorithms and rigorous error analyses have been developed to refine and expand upon the original MBO method [17, 38, 39]. For instance, in [23], the authors extend the MBO method to multiphase volume-constrained curvature motion using an auction dynamics scheme. This extension allows for solving problems related to minimal surface area with multiphase volume constraints.

In this paper, two new iterative methods are introduced for longest minimal length partitions. The objective functional is approximated by a short time heat flow. Then, the method of threshold dynamics is used to maximize $PI(\Omega, \mathbf{c})$ under volume constraints, and auction dynamics is used to find $SP(\Omega, \mathbf{c})$ for a fixed Ω .

The rest of this paper is organized as follows. Section 2 introduces approximations for the objective functional. These approximations serve as the foundation for the subsequent methods. Section 3 presents the derivation of the two-step methods based on the introduced approximations. In Section 4, we present numerical experiments in two and three dimensions to demonstrate the performance of the proposed methods. We propose in Section 5 an objective functional-monotone method. We then draw conclusions and discussions in Section 6.

2. Approximations of the objective functional

Let $\Omega \subset \mathbb{R}^d$ be an open and connected set to be partitioned. We define the objective functional (the length of the partition of Ω) by

$$E(\Omega, (\omega_i)_{i=1}^n) = \sum_{i=1}^n \text{Per}_\Omega(\omega_i). \quad (2)$$

Given a volume constraint $V > 0$ and partition proportions $\mathbf{c} = (c_1, \dots, c_n)$, the relative isoperimetric profile is written as

$$PI(\Omega, \mathbf{c}) = \min_{|\omega_i|=c_i V} E(\Omega, (\omega_i)_{i=1}^n).$$

The longest minimal length problem can be formulated as the following max-min optimization problem

$$\max_{|\Omega|=V} PI(\Omega, \mathbf{c}) = \max_{|\Omega|=V} \min_{|\omega_i|=c_i V} E(\Omega, (\omega_i)_{i=1}^n). \quad (3)$$

To approximate the objective functional, we use indicator functions to implicitly represent the regions Ω and $(\omega_i)_{i=1}^n$. Define u_Ω and $(u_i)_{i=1}^n$ by

$$u_\Omega(\mathbf{x}) = \begin{cases} 1 & \text{if } \mathbf{x} \in \Omega, \\ 0 & \text{if } \mathbf{x} \notin \Omega, \end{cases} \quad u_i(\mathbf{x}) = \begin{cases} 1 & \text{if } \mathbf{x} \in \omega_i, \\ 0 & \text{if } \mathbf{x} \notin \omega_i, \end{cases} \quad \text{for } i = 1, \dots, n. \quad (4)$$

The volume constraints in (3) can be expressed as $\int_{\mathbb{R}^d} u_\Omega d\mathbf{x} = V$ and $\int_{\mathbb{R}^d} u_i d\mathbf{x} = c_i V$. Since $(\omega_i)_{i=1}^n$ is a partition of Ω , we also have $\sum_{i=1}^n u_i = u_\Omega$.

To approximate the objective functional, instead of using a Modica-Mortola approximation as in [12], we use indicator functions and Gaussian convolution. Note that $\text{Per}_\Omega(\omega_i) = \sum_{j=1}^n \text{Per}_{\omega_i \cup \omega_j}(\omega_i)$, and $\text{Per}_{\omega_i \cup \omega_j}(\omega_i) = \text{Per}_{\omega_i}(\omega_i) = 0$. For any $i \neq j$, we have $\text{Per}_{\omega_i \cup \omega_j}(\omega_j) = \text{Per}_{\omega_i \cup \omega_j}(\omega_i)$, which can be approximated by

$$\text{Per}_{\omega_i \cup \omega_j}(\omega_j) \approx \sqrt{\frac{\pi}{\tau}} \int_{\mathbb{R}^d} u_i (G_\tau * u_j) d\mathbf{x}, \quad (5)$$

where

$$G_\tau(\mathbf{x}) = \frac{1}{(4\pi\tau)^{d/2}} \exp\left(-\frac{|\mathbf{x}|^2}{4\tau}\right)$$

is the Gaussian kernel and $*$ denotes convolution in \mathbb{R}^d . The convergence of this approximation for closed curves has been shown in [14] as τ goes to 0^+ and the multi-phase formula was proposed in [20]. By utilizing (5), we approximate $E(\Omega, (\omega_i)_{i=1}^n)$ in (2) by

$$\begin{aligned} E(\Omega, (\omega_i)_{i=1}^n) &= \sum_{i=1}^n \sum_{j \neq i} \text{Per}_{\omega_j \cup \omega_i}(\omega_i) \\ &\approx \sqrt{\frac{\pi}{\tau}} \sum_{i=1}^n \sum_{j \neq i} \int_{\mathbb{R}^d} u_i (G_\tau * u_j) d\mathbf{x} \end{aligned} \quad (6)$$

$$\begin{aligned} &= \sqrt{\frac{\pi}{\tau}} \sum_{i=1}^n \int_{\mathbb{R}^d} u_i \left(G_\tau * \left(\sum_{j \neq i} u_j \right) \right) d\mathbf{x} \\ &= \sqrt{\frac{\pi}{\tau}} \sum_{i=1}^n \int_{\mathbb{R}^d} u_i (G_\tau * (u_\Omega - u_i)) d\mathbf{x} \\ &= \sqrt{\frac{\pi}{\tau}} \sum_{i=1}^n \int_{\mathbb{R}^d} (G_{\tau/2} * u_i) (G_{\tau/2} * (u_\Omega - u_i)) d\mathbf{x}. \end{aligned} \quad (7)$$

Since $\sqrt{\frac{\pi}{\tau}}(G_{\tau/2} * u_i) (G_{\tau/2} * (u_\Omega - u_i))$ concentrates on Ω as τ goes to 0^+ , *i.e.*,

$$\lim_{\tau \rightarrow 0^+} \sqrt{\frac{\pi}{\tau}} \int_{\mathbb{R}^d \setminus \Omega} (G_{\tau/2} * u_i) (G_{\tau/2} * (u_\Omega - u_i)) \, d\mathbf{x} = 0,$$

when τ is sufficiently small, the objective functional will not change too much if we replace the integrating domain in (7) from \mathbb{R}^d to Ω . To achieve this, recall that u_Ω is the indicator function of Ω , we multiply the integrand in (7) by u_Ω . Thus the objective functional in (7) is further approximated by

$$\begin{aligned} (7) &\approx \sqrt{\frac{\pi}{\tau}} \sum_{i=1}^n \int_{\mathbb{R}^d} u_\Omega (G_{\tau/2} * u_i) (G_{\tau/2} * (u_\Omega - u_i)) \, d\mathbf{x} \\ &= \sqrt{\frac{\pi}{\tau}} \int_{\mathbb{R}^d} u_\Omega \left(S_{\tau/2} - \sum_{i=1}^n (G_{\tau/2} * u_i)^2 \right) \, d\mathbf{x} \\ &\quad - \sqrt{\frac{\pi}{\tau}} \int_{\mathbb{R}^d} u_\Omega S_{\tau/2} (G_{\tau/2} * (1 - u_\Omega)) \, d\mathbf{x}, \end{aligned} \quad (8)$$

where $S_{\tau/2}$ denotes $S_{\tau/2}(\mathbf{x}) := G_{\tau/2} * (\sum_{i=1}^n u_i)(\mathbf{x})$. By [40], in the sense of τ going to 0^+ , the last quadratic term can be approximated by

$$\begin{aligned} &\sqrt{\frac{\pi}{\tau}} \int_{\mathbb{R}^d} u_\Omega S_{\tau/2} (G_{\tau/2} * (1 - u_\Omega)) \, d\mathbf{x} \\ &\approx \sqrt{\frac{\pi}{\tau}} \int_{\mathbb{R}^d} u_\Omega S_{\tau/2}^{\frac{1}{2}} \left(G_{\tau/2} * \left(S_{\tau/2}^{\frac{1}{2}} (1 - u_\Omega) \right) \right) \, d\mathbf{x}. \end{aligned}$$

Denote the approximate objective functional by

$$\begin{aligned} \tilde{E}_\tau(u_\Omega, (u_i)_{i=1}^n) &:= \sqrt{\frac{\pi}{\tau}} \int_{\mathbb{R}^d} u_\Omega \left(S_{\tau/2} - \sum_{i=1}^n (G_{\tau/2} * u_i)^2 \right) \, d\mathbf{x} \\ &\quad - \sqrt{\frac{\pi}{\tau}} \int_{\mathbb{R}^d} u_\Omega S_{\tau/2}^{\frac{1}{2}} \left(G_{\tau/2} * \left(S_{\tau/2}^{\frac{1}{2}} (1 - u_\Omega) \right) \right) \, d\mathbf{x}. \end{aligned} \quad (9)$$

The original problem (3) is approximated by

$$\begin{aligned} &\max_{\substack{u_\Omega \in \mathcal{B} \\ \int_{\mathbb{R}^d} u_\Omega \, d\mathbf{x} = V}} \min_{\substack{u_i \in \mathcal{B} \\ \sum u_i = u_\Omega}} \tilde{E}_\tau(u_\Omega, (u_i)_{i=1}^n), \end{aligned} \quad (10)$$

where $\mathcal{B} := \{u \in BV(\Omega, \mathbb{R}) \mid u = \{0, 1\}\}$, and $BV(\Omega, \mathbb{R})$ denotes the bounded-variation functional space.

Note that (6) can also be used for approximation, leading to another approximation of the objective functional

$$\hat{E}_\tau(u_\Omega, (u_i)_{i=1}^n) := \sqrt{\frac{\pi}{\tau}} \sum_{i=1}^n \sum_{j \neq i} \int_{\mathbb{R}^d} u_i (G_\tau * u_j) \, d\mathbf{x}. \quad (11)$$

The corresponding modified problem is

$$\begin{aligned} &\max_{\substack{u_\Omega \in \mathcal{B} \\ \int_{\mathbb{R}^d} u_\Omega \, d\mathbf{x} = V}} \min_{\substack{u_i \in \mathcal{B} \\ \sum u_i = u_\Omega}} \hat{E}_\tau(u_\Omega, (u_i)_{i=1}^n). \end{aligned} \quad (12)$$

Here, \tilde{E}_τ and \hat{E}_τ are equivalent to each other in the sense of τ converging to 0^+ , and hence are (10) and (12).

3. Derivation of the methods

Based on the two objective functional approximations in (9) and (11), in this section, two iterative methods are derived for longest minimal length partitions. Denote the indicator functions of the total region and the shortest partition in k -th iteration by u_Ω^k and $(u_i^k)_{i=1}^n$ respectively. Each method contains two steps:

Step 1: Fix $(u_i^k)_{i=1}^n$ and find u_Ω^{k+1} by maximizing \tilde{E}_τ .

Step 2: Fix u_Ω^{k+1} and find $(u_i^{k+1})_{i=1}^n$ by minimizing \hat{E}_τ .

In Step 2, due to the good form of \hat{E}_τ , auction dynamics [23] can be directly employed in both methods. The $(u_i^k)_{i=1}^n$ given by the two methods preserve $\sum_{i=1}^n u_i^k = u_\Omega^k$ to ensure that the collection of subsets is a partition of the total region. In Step 1, the update is based on the objective functional \tilde{E}_τ and threshold dynamics is used. The constraint $\sum_{i=1}^n u_i = u_\Omega$ is relaxed in this part to update the total region. Otherwise, if $u_\Omega^{k+1} = \sum_{i=1}^n u_i^k = u_\Omega^k$, the total region would remain unchanged during iterations. To maintain the stability of the method, in the first method, the update of u_Ω^{k+1} is fully led by the behavior of \tilde{E}_τ , while $(u_i^{k+1})_{i=1}^n$ are updated by running auction dynamics several times to avoid local minimizer of \tilde{E}_τ . In the second method, a proximal term is introduced to control the evolution of u_Ω and only a one-time auction dynamics is used to updated $(u_i^{k+1})_{i=1}^n$, which enhance both the stability and efficiency.

3.1. The first method

3.1.1. Update of u_Ω^{k+1}

In this step, we find u_Ω^{k+1} based on $(u_i^k)_{i=1}^n$. In the update of the total region, the approximate objective functional \tilde{E}_τ (defined in (9)) serves as a guidance. Fixing $(u_i^k)_{i=1}^n$, we update u_Ω^{k+1} by

$$u_\Omega^{k+1} = \arg \max_{\substack{u_\Omega \in \mathcal{B} \\ \int_{\mathbb{R}^d} u_\Omega dx = V}} \tilde{E}_\tau(u_\Omega, (u_i^k)_{i=1}^n). \quad (13)$$

To solve (13), we relax the constraint $u_\Omega \in \{0, 1\}$ to $u_\Omega \in [0, 1]$. Specifically, we define $\mathcal{K} := \{u \in BV(\Omega, \mathbb{R}) | u \in [0, 1]\}$ and consider the following problem instead:

$$u_\Omega^{k+1} = \arg \max_{\substack{u_\Omega \in \mathcal{K} \\ \int_{\mathbb{R}^d} u_\Omega dx = V}} \tilde{E}_\tau(u_\Omega, (u_i^k)_{i=1}^n). \quad (14)$$

The following lemma shows that (13) and (14) have the same maximizer.

Lemma 3.1. *The problems (13) and (14) have the same maximizer, i.e.,*

$$\arg \max_{\substack{u_\Omega \in \mathcal{B} \\ \int_{\mathbb{R}^d} u_\Omega dx = V}} \tilde{E}_\tau(u_\Omega, (u_i^k)_{i=1}^n) = \arg \max_{\substack{u_\Omega \in \mathcal{K} \\ \int_{\mathbb{R}^d} u_\Omega dx = V}} \tilde{E}_\tau(u_\Omega, (u_i^k)_{i=1}^n).$$

Proof. Note that

$$\max_{\substack{u_\Omega \in \mathcal{B} \\ \int_{\mathbb{R}^d} u_\Omega dx = V}} \tilde{E}_\tau(u_\Omega, (u_i^k)_{i=1}^n) \leq \max_{\substack{u_\Omega \in \mathcal{K} \\ \int_{\mathbb{R}^d} u_\Omega dx = V}} \tilde{E}_\tau(u_\Omega, (u_i^k)_{i=1}^n),$$

since $\mathcal{B} \subset \mathcal{K}$. To prove the equivalence, it suffices to show

$$\arg \max_{\substack{u_\Omega \in \mathcal{K} \\ \int_{\mathbb{R}^d} u_\Omega d\mathbf{x} = V}} \tilde{E}_\tau(u_\Omega, (u_i^k)_{i=1}^n) \in \left\{ u_\Omega \in \mathcal{B} : \int_{\mathbb{R}^d} u_\Omega d\mathbf{x} = V \right\}.$$

Assume this is not true and the maximizer is u^* . Then there exists a set $A \subset \Omega$ with $|A| > 0$ and $0 < c < \frac{1}{2}$ such that

$$u^*(\mathbf{x}) \in (c, 1 - c), \text{ for any } \mathbf{x} \in \Omega.$$

Divide A into two subsets A_1 and A_2 such that $A_1 \cup A_2 = A$, $A_1 \cap A_2 = \emptyset$ and $|A_1| = |A_2| = \frac{1}{2}|A|$. Define $u^t = u^* + t\chi_{A_1} - t\chi_{A_2}$ where χ_{A_1} and χ_{A_2} are indicator functions of A_1 and A_2 respectively. Then $u^t \in \{u_\Omega \in \mathcal{K} : \int u_\Omega d\mathbf{x} = V\}$ for any $|t| < \frac{c}{2}$. Observe that

$$\begin{aligned} & \frac{d^2}{dt^2} \tilde{E}_\tau(u^t, (u_i^k)_{i=1}^n) \\ &= 2\sqrt{\frac{\pi}{\tau}} \int_{\mathbb{R}^d} (\chi_{A_1} - \chi_{A_2})(S_{\tau/2}^k)^{\frac{1}{2}} \left(G_{\tau/2} * \left((\chi_{A_1} - \chi_{A_2})(S_{\tau/2}^k)^{\frac{1}{2}} \right) \right) d\mathbf{x} \\ &= 2\sqrt{\frac{\pi}{\tau}} \int_{\mathbb{R}^d} \left(G_{\tau/4} * \left((\chi_{A_1} - \chi_{A_2})(S_{\tau/2}^k)^{\frac{1}{2}} \right) \right)^2 d\mathbf{x} \\ &> 0, \end{aligned}$$

where $S_{\tau/2}^k$ denotes $S_{\tau/2}^k(\mathbf{x}) = G_{\tau/2} * (\sum_{i=1}^n u_i^k)(\mathbf{x})$. Particularly, when taking $t = 0$, $u^0 = u^*$, $\frac{d^2}{dt^2} \tilde{E}_\tau(u^*, (u_i^k)_{i=1}^n) > 0$, which contradicts with that u^* is the maximizer. Therefore, the maximizer is in \mathcal{B} and this ends the proof. \square

By Lemma 3.1, solving (13) is converted to solving (14), for which we follow [20] to linearize $\tilde{E}_\tau(u_\Omega, (u_i^k)_{i=1}^n)$ as

$$L_\tau(u_\Omega, u_\Omega^k, (u_i^k)_{i=1}^n) = \int_{\mathbb{R}^d} u_\Omega \phi^k d\mathbf{x},$$

where the dominant function is

$$\phi^k(\mathbf{x}) = \sqrt{\frac{\pi}{\tau}} \left(S_{\tau/2}^k - \sum_{i=1}^n \left(G_{\tau/2} * u_i^k \right)^2 + (S_{\tau/2}^k)^{\frac{1}{2}} G_{\tau/2} * \left((S_{\tau/2}^k)^{\frac{1}{2}} (2u_\Omega^k - 1) \right) \right). \quad (15)$$

By threshold dynamics, u_Ω^{k+1} is updated by maximizing the linearized objective functional under the volume constraint

$$u_\Omega^{k+1} = \arg \max_{\int_{\mathbb{R}^d} u_\Omega d\mathbf{x} = V} L_\tau(u_\Omega, u_\Omega^k, (u_i^k)_{i=1}^n).$$

Let $\sigma > 0$ such that

$$\int_{\mathbb{R}^d} \chi_\sigma(\mathbf{x}) d\mathbf{x} = V, \quad (16)$$

where $\chi_\sigma(\mathbf{x})$ is the indicator function of the set $\{\mathbf{x} \in \mathbb{R}^d : \phi^k(\mathbf{x}) \geq \sigma\}$. It is easy to see that the maximizer u_Ω^{k+1} is determined point-wisely by

$$u_\Omega^{k+1}(\mathbf{x}) = \begin{cases} 1 & \text{if } \phi^k(\mathbf{x}) \geq \sigma, \\ 0 & \text{if } \phi^k(\mathbf{x}) < \sigma, \end{cases} \quad (17)$$

which is exactly $u_\Omega^{k+1}(\mathbf{x}) = \chi_\sigma(\mathbf{x})$.

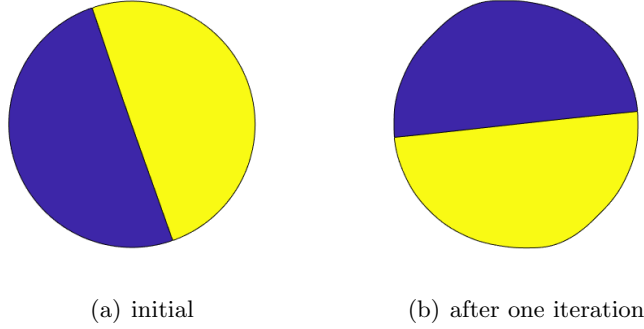


Figure 2: The initial condition is a disc. After one iteration by (17), the total region changes instead of remaining round.

Remark 3.2. In [12], during the update of Fourier coefficients of the radial function which represents the total region, the volume constraint is broken. Then the authors project the updated coefficients onto the volume constraint using a homothety. For the methods in this paper, volume preserving is kept in the way of (16) and (17). For regular discretization, such a σ is easy to find. Besides, since σ is a threshold of the dominant function, it makes sure that the update maximizes the approximate objective functional in this time step under the volume constraint.

In fact, if we just update the total region by (17) in each iteration, u_{Ω}^{k+1} will not converge to a stationary point, and the iterations will not stop. This is because the update of u_{Ω}^{k+1} depends on $(u_i^k)_{i=1}^n$, which represents a shortest partition of u_{Ω}^k but may not be unique. For example, each diameter of a disc gives a shortest partition in the two-dimensional bisection case, and there are infinity many diameters. When we update the total region, u_{Ω}^{k+1} differs from u_{Ω}^k in the direction of increasing the objective functional of $(u_i^k)_{i=1}^n$. However, this may decrease the objective functional of other shortest partitions and eventually decrease the objective function we want to maximize. As Figure 2 shows, if we take a disc as the initial total region, the update by (17) will give a region which is not a disc after one iteration. This contradicts with the analytical result in [7] that the disc is the optimal solution of bisection in the two-dimensional case.

To address this issue, one approach is to identify all the shortest partitions of u_{Ω}^k , and then update the total region in the direction of increasing the objective functional of all of them. However, this is impractical to implement as the number of shortest partitions can be infinite. An alternative approach is to reduce the update rate gradually when the change of objective functional is small. Then when u_{Ω}^k is close to the optimal solution, it will not change too much and go far away.

Instead of using all the points in the level set $\{\mathbf{x} \in \mathbb{R}^d : \phi^k(\mathbf{x}) \geq \sigma\}$, we only use a part of it during the update of the total region. Denote $0 \leq \beta \leq 1$ the update step-length, and $u_{\Omega}^{process}(\mathbf{x}) = \chi_{\sigma}(\mathbf{x})$ the indicator function obtained by (17). Denote $\Omega_{process}$ the region corresponding to $u_{\Omega}^{process}$, $A = \Omega_{process} - \Omega^k$ and $B = \Omega^k - \Omega_{process}$. Intuitively speaking, to increase the approximate objective functional in the direction of $(u_i^k)_{i=1}^n$, the original algorithm tends to delete the points in B and add the points in A into the total region. Since $|\Omega_{process}| = |\Omega^k|$ by volume conservation, $|A| = |B|$ and $A \cap B = \emptyset$. In order to reduce the update rate, we find σ_1, σ_2 such that

$$\begin{aligned} \int_A \chi_{\sigma_1}(\mathbf{x}) d\mathbf{x} &= \beta|A|, \\ \int_B \chi_{\sigma_2}(\mathbf{x}) d\mathbf{x} &= (1 - \beta)|B|, \end{aligned}$$

and define $\tilde{A} = \{x \in A : \phi^k(\mathbf{x}) \geq \sigma_1\}$ and $\tilde{B} = \{x \in B : \phi^k(\mathbf{x}) \leq \sigma_2\}$. Then \tilde{A} is a subset of A with $|\tilde{A}| = \beta|A|$, and for any $\mathbf{x}_1 \in \tilde{A}$, $\mathbf{x}_2 \in (A - \tilde{A})$, we have

$$\phi^k(\mathbf{x}_1) \geq \sigma_1 > \phi^k(\mathbf{x}_2),$$

which means \tilde{A} is the part of A with higher dominant function values. Similarly, $|\tilde{B}| \subset |B|$, $|\tilde{B}| = \beta|B|$ and \tilde{B} is the part of B with lower dominant function values. We update the total region by

$$u_\Omega^{k+1}(\mathbf{x}) = u_\Omega^k(\mathbf{x}) + \chi_{\tilde{A}} - \chi_{\tilde{B}}, \quad (18)$$

where $\chi_{\tilde{A}}$ and $\chi_{\tilde{B}}$ are the indicator functions of \tilde{A} and \tilde{B} . In other words, we delete the points in \tilde{B} and add the points in \tilde{A} into the total region, instead of the whole B and A . Note that $|\tilde{A}| = |\tilde{B}|$ and $\tilde{A} \cap \tilde{B} = \emptyset$. The update of the total region follows volume conservation. Here β controls the degree of differences between u_Ω^k and u_Ω^{k+1} . When $\beta = 0$, the total region will not update during iterations; when $\beta = 1$, the update is the same as (17). Now the update step-length can be controlled by setting different value of β .

When β is large, u_Ω^k may be difficult to converge due to the non-uniqueness of the solution and the two-step updating strategy. In fact, it oscillates around a disc. To obtain a stable and convergent scheme, we need to control the updating rate of u_Ω^k , which is β here. For a fixed β , after sufficiently many iterations, even though u_Ω^k oscillates, its objective functional stays at a certain scale. To evaluate the change of objective functional during iterations, we calculate the change of averaged objective functional over a few (M in Algorithm 3) consecutive iterations. When the change is less than a tolerance r_{tol} , it is regarded to be small, and we reduce β by multiplying a factor γ ($0 < \gamma < 1$). Here the averaged objective functional of a few steps is used instead of the objective functional in one iteration. This can mitigate the impact of local shortest partitions on objective functional calculation.

3.1.2. Update of $(u_i^{k+1})_{i=1}^n$

In the update of shortest partition, we fix u_Ω^{k+1} and use the approximate objective functional \hat{E}_τ defined in (11). Functions $(u_i^{k+1})_{i=1}^n$ are computed by solving

$$(u_i^{k+1})_{i=1}^n = \underset{\substack{u_i \in \mathcal{B} \\ \int_{\mathbb{R}^d} u_i d\mathbf{x} = c_i V \\ \sum u_i = u_\Omega^{k+1}}}{\arg \min} \hat{E}_\tau(u_\Omega^{k+1}, (u_i)_{i=1}^n). \quad (19)$$

Observe that \hat{E}_τ is proportional to the heat content energy in [23]

$$HC_\tau = \frac{1}{\sqrt{\tau}} \sum_{i \neq j} \int u_i(\mathbf{x})(G_\tau * u_j)(\mathbf{x}) d\mathbf{x}. \quad (20)$$

Therefore, given u_Ω^{k+1} with parameters of stopping criterion $\boldsymbol{\mu}$, auction dynamics with volume constraints from [23] directly finds a shortest partition $(u_i^{k+1})_{i=1}^n$. Here $\boldsymbol{\mu} = (m, \epsilon_{min}, \alpha, \epsilon_0)$, m is the number of maximum steps, ϵ_{min} is the auction error tolerance, α is the epsilon scaling factor and ϵ_0 is the initial epsilon value. Denote the auction dynamics method by *ADM*. We compute $(u_i^{k+1})_{i=1}^n$ as

$$(u_i^{k+1})_{i=1}^n = ADM(u_\Omega^{k+1}, V, \mathbf{c}, \tau; \boldsymbol{\mu}), \quad (21)$$

where details of ADM is summarized in Algorithm 1, with the sub-routine membership auction summarized in Algorithm 2.

Algorithm 1: Auction dynamics

Input: Discrete total region u_Ω , volume constraint V , partition proportions \mathbf{c} , time step τ , parameters of stop conditions $\boldsymbol{\mu} = (m, \epsilon_{min}, \alpha, \epsilon_0)$.

Output: Shortest partitions $(u_i)_{i=1}^n$.

```
1 Set  $l = 0$ ; initialize  $(u_{i,0})_{i=1}^n$  randomly with  $\int u_{i,0} d\mathbf{x} = c_i V$ ; set  $\bar{\epsilon} = \epsilon/n$ ; compute  $G_\tau$ ;  
2 while  $l < m$  and not converged do  
3   Compute the convolutions:  $\psi_i^l(\mathbf{x}) = \sum_{i \neq j} (G_\tau * u_{j,l})(\mathbf{x})$ ;  
4   Compute the assignment problem coefficients:  $\mathbf{a}^l = 1 - \boldsymbol{\psi}^l$ ;  
5   Initialize the prices  $\mathbf{p} = \mathbf{0}$ , and  $\epsilon = \epsilon_0$ ;  
6   while  $\epsilon \geq \bar{\epsilon}$  do  
7     Run Algorithm 2:  $((u_i^{out})_{i=1}^n, \mathbf{p}^{out}) = \text{Membership auction}(\epsilon, V\mathbf{c}, \mathbf{a}^l, \mathbf{p}, u_\Omega)$ ;  
8     Set  $\mathbf{p} = \mathbf{p}^{out}$ ;  
9     Divide  $\epsilon$  by  $\alpha$ ;  
10    if  $\epsilon < \bar{\epsilon}$  then  
11      | Set  $(u_{i,l+1})_{i=1}^n = (u_i^{out})_{i=1}^n$ ;  
12    end  
13  end  
14  Set  $l = l + 1$ ;  
15 end  
16 Return  $(u_i)_{i=1}^n = (u_{i,l})_{i=1}^n$ 
```

Remark 3.3. In Algorithm 1, $\boldsymbol{\psi}^l$ is a tensor whose i -th element is $\psi_i^l(\mathbf{x})$. After discretizing the space, it becomes a matrix. The criterion for convergence is $u_{i,l+1}(\mathbf{x}) = u_{i,l}(\mathbf{x})$ for all $i = 1, \dots, n$, i.e., when the partitions are no longer updated. In Algorithm 2, $i_{cs}(\mathbf{x}, \mathbf{p})$ and $i_{next}(\mathbf{x}, \mathbf{p}, i^*)$ are defined by

$$i_{cs}(\mathbf{x}, \mathbf{p}) = \arg \max_{1 \leq i \leq n} [a_i(\mathbf{x}) - p_i], \quad i_{next}(\mathbf{x}, \mathbf{p}, i^*) \in \arg \max_{j \neq i^*} [a_j(\mathbf{x}) - p_j].$$

Here $i_{cs}(\mathbf{x}, \mathbf{p})$ is a set containing all indices satisfying the right-hand side, $i_{next}(\mathbf{x}, \mathbf{p}, i^*)$ is just an arbitrary element of the set satisfying the right-hand side.

The results of ADM critically depends on its initialization, which is usually set as random. In many cases, ADM does not always give global shortest partitions, but a local one. To make the partitions more likely to be a global shortest one, in the first method, ADM is repeated several times in each iteration. Every time a random initialization is given and a corresponding partition is created, we compute the objective functional of all partitions. The partitions with minimal objective functional are regarded as the shortest partitions. This increases the stability of the method.

The first two-step iterative method for the longest minimal length partitions problem is summarized in Algorithm 3. The stopping criterion is set to be $\beta < \beta_{min}$ for some constant β_{min} , or the total regions between two iterations are exactly the same.

Remark 3.4. In Algorithm 3 and Algorithm 4, convergence means $u_\Omega^{k+1} = u_\Omega^k$.

Remark 3.5. In Algorithm 3, although ADM is repeated with the same parameters, the random initialization makes the output $(u_{i,q}^{k+1})_{i=1}^n$ different each time.

Algorithm 2: Membership auction

Input: $\epsilon > 0$, volumes \mathbf{V} , coefficients \mathbf{a} , initial prices \mathbf{p}^0 and indicator function $u_\Omega(\mathbf{x})$.

Output: Final partitions and prices $((u_i)_{i=1}^n, \mathbf{p})$.

```

1 For every  $i \in \{1, \dots, n\}$  set  $u_i(\mathbf{x}) = 0$  for all  $\mathbf{x}$  such that  $u_\Omega(\mathbf{x}) = 1$ ; set  $\mathbf{p} = \mathbf{p}^0$ 
2 while some  $\mathbf{x}$  is unassigned, i.e.,  $u_\Omega(\mathbf{x}) = 1$  but  $\sum_i u_i(\mathbf{x}) = 0$ , do
3   for each unassigned  $\mathbf{x}$  do
4     Compute  $i_{cs}(\mathbf{x}, \mathbf{p})$  and choose one element  $i^* \in i_{cs}(\mathbf{x}, \mathbf{p})$ ;
5     Set  $b(\mathbf{x}) = p_{i^*} + \epsilon + (a_{i^*}(\mathbf{x}) - p_{i^*}) - (a_{i_{next}(\mathbf{x}, \mathbf{p}, i^*)}(\mathbf{x}) - p_{i_{next}(\mathbf{x}, \mathbf{p}, i^*)})$ ;
6     if  $\int u_{i^*} d\mathbf{x} = V_{i^*}$  then
7       Find  $\mathbf{y} = \arg \min_{u_{i^*}(\mathbf{z})=1} b(\mathbf{z})$ ;
8       Set  $u_{i^*}(\mathbf{y}) = 0$  and  $u_{i^*}(\mathbf{x}) = 1$ ;
9       Set  $p_{i^*} = \min_{u_{i^*}(\mathbf{z})=1} b(\mathbf{z})$ ;
10    else
11      Set  $u_{i^*}(\mathbf{x}) = 1$ ;
12      if  $\int u_{i^*} d\mathbf{x} = V_{i^*}$  then
13        Set  $p_{i^*} = \min_{u_{i^*}(\mathbf{z})=1} b(\mathbf{z})$ ;
14      end
15    end
16  end
17 end
18 Return  $((u_i)_{i=1}^n, \mathbf{p})$ 

```

3.2. The second method

In the first method, to increase the stability, ADM is repeated several times in one iteration to find the shortest partitions. However, this increases the time complexity. To address this issue, the second method uses a more efficient way for stability. In the updating of $(u_i^k)_{i=1}^n$, the second method follows a similar process as the first method but only employs ADM once. We omit the details here. In the updating of u_Ω^{k+1} , a regularization term is introduced.

3.2.1. Update of u_Ω^{k+1} by $(u_i^k)_{i=1}^n$

In the update of the total region, the approximate objective functional \tilde{E}_τ in (9) is used. Given u_Ω^k and $(u_i^k)_{i=1}^n$, u_Ω^{k+1} is attained by

$$u_\Omega^{k+1} = \arg \max_{\substack{u_\Omega \in \mathcal{B} \\ \int u_\Omega = V}} \tilde{E}_\tau(u_\Omega, (u_i^k)_{i=1}^n) + \lambda \int_{\mathbb{R}^d} u_\Omega G_{\tau'} * \left(\sum_{i=1}^n u_i^k \right) d\mathbf{x}, \quad (22)$$

where $\lambda > 0, \tau' > 0$. In (22), the second term is a regularization term to relax the constraint of $\sum_{i=1}^n u_i = u_\Omega$ and ensure that u_Ω^{k+1} does not deviate significantly from u_Ω^k . In the following, we denote the regularized objective functional as

$$\tilde{E}_{\tau, \tau'}^\lambda(u_\Omega, (u_i^k)_{i=1}^n) = \tilde{E}_\tau(u_\Omega, (u_i^k)_{i=1}^n) + \lambda \int_{\mathbb{R}^d} u_\Omega G_{\tau'} * \left(\sum_{i=1}^n u_i^k \right) d\mathbf{x}.$$

In fact, (22) is a discretized scheme for an evolution equation of u_Ω . Based on (9), u_Ω^{k+1} is

Algorithm 3: The first method for longest minimal length partitions

Input: Volume constraint V , partition proportions $\mathbf{c} = (c_1, \dots, c_n)$ satisfying $c_i > 0$ and $\sum_{i=1}^n c_i = 1$, time step $\tau > 0$, auction dynamics parameters $\boldsymbol{\mu}$, repeat times of auction dynamics p , update step-length parameters $0 \leq \beta_0 \leq 1, 0 < \gamma < 1$, the number of steps in average objective functional $M \in \mathbb{N}$, $r_{tol} > 0$, $0 < \beta_{min} < 1$.

Output: u_Ω maximizing the objective functional, shortest partitions $(u_i)_{i=1}^n$.

```

1 Set  $k = 0$ ; initialize  $u_\Omega^0$  randomly with  $\int u_\Omega^0 d\mathbf{x} = V$ ;  $\beta = \beta_0$ ;
2 for  $1 \leq q \leq p$  do
3   | Compute  $(u_{i,q}^0)_{i=1}^n = ADM(u_\Omega^0, V, \mathbf{c}, \tau; \boldsymbol{\mu})$ ;
4 end
5 Set  $(u_i^0)_{i=1}^n = \arg \min_{(u_{i,q}^0)_{i=1}^n} \tilde{E}_\tau(u_\Omega^0, (u_{i,q}^0)_{i=1}^n)$ ;
6 while  $\beta > \beta_{min}$  and not converge do
7   | Compute dominant function  $\phi^k$  by (15);
8   | Update  $u_\Omega^{k+1}$  by (18) using  $\beta$ ;
9   | for  $1 \leq q \leq p$  do
10    | Compute  $(u_{i,q}^{k+1})_{i=1}^n = ADM(u_\Omega^{k+1}, V, \mathbf{c}, \tau; \boldsymbol{\mu})$ ;
11    end
12    Set  $(u_i^{k+1})_{i=1}^n = \arg \min_{(u_{i,q}^{k+1})_{i=1}^n} \tilde{E}_\tau(u_\Omega^{k+1}, (u_{i,q}^{k+1})_{i=1}^n)$ ;
13    if  $k > M$  then
14      | Compute  $E_{ave}^k = \frac{1}{M} \sum_{j=k-M+1}^k \tilde{E}_\tau(u_\Omega^j, (u_i^j)_{i=1}^n)$ ;
15      | Compute  $E_{ave}^{k+1} = \frac{1}{M} \sum_{j=k-M+2}^{k+1} \tilde{E}_\tau(u_\Omega^j, (u_i^j)_{i=1}^n)$ ;
16      | if  $|E_{ave}^{k+1} - E_{ave}^k| / |E_{ave}^{k+1}| < r_{tol}$  then
17        |  $\beta = \gamma\beta$ ;
18        end
19      end
20       $k = k + 1$ ;
21 end
22 Return  $u_\Omega = u_\Omega^k$ ,  $(u_i)_{i=1}^n = (u_i^k)_{i=1}^n$ 

```

expected to maximize $\tilde{E}_\tau(u_\Omega, (u_i^k)_{i=1}^n)$. Consider a gradient ascent flow:

$$\frac{\partial u_\Omega}{\partial t} - \partial \tilde{E}_\tau(u_\Omega, (u_i^k)_{i=1}^n) = 0. \quad (23)$$

We update u_Ω^{k+1} by solving (23) by a short time (one time step), and discretize (23) with the time step $1/\lambda$ by a backward Euler scheme:

$$\frac{u_\Omega^{k+1} - u_\Omega^k}{1/\lambda} - \partial \tilde{E}_\tau(u_\Omega^{k+1}, (u_i^k)_{i=1}^n) = 0. \quad (24)$$

Then u_Ω^{k+1} solves

$$\begin{aligned}
u_\Omega^{k+1} &= \arg \min_{u_\Omega} \left[\frac{\lambda}{2} \int_{\mathbb{R}} |u_\Omega - u_\Omega^k|^2 d\mathbf{x} - \tilde{E}_\tau(u_\Omega, (u_i^k)_{i=1}^n) \right] \\
&= \arg \max_{u_\Omega} \left[\tilde{E}_\tau(u_\Omega, (u_i^k)_{i=1}^n) - \frac{\lambda}{2} \int_{\mathbb{R}} |u_\Omega - u_\Omega^k|^2 d\mathbf{x} \right] \\
&= \arg \max_{u_\Omega} \left[\tilde{E}_\tau(u_\Omega, (u_i^k)_{i=1}^n) - \frac{\lambda}{2} \int_{\mathbb{R}} \left((u_\Omega)^2 + (u_\Omega^k)^2 - 2u_\Omega u_\Omega^k \right) d\mathbf{x} \right]. \tag{25}
\end{aligned}$$

Using the constraint $u_\Omega \in \mathcal{B}$, $\int_{\mathbb{R}} u_\Omega d\mathbf{x} = V$ and the fact $u_\Omega^k \in \mathcal{B}$, $\int_{\mathbb{R}} u_\Omega^k d\mathbf{x} = V$, we further deduce

$$\begin{aligned}
u_\Omega^{k+1} &= \arg \max_{u_\Omega} \left[\tilde{E}_\tau(u_\Omega, (u_i^k)_{i=1}^n) - \frac{\lambda}{2} \int_{\mathbb{R}} \left(u_\Omega + u_\Omega^k - 2u_\Omega u_\Omega^k \right) d\mathbf{x} \right] \\
&= \arg \max_{u_\Omega} \left[\tilde{E}_\tau(u_\Omega, (u_i^k)_{i=1}^n) - \frac{\lambda}{2} \int_{\mathbb{R}} \left(-2u_\Omega u_\Omega^k \right) d\mathbf{x} \right] - \lambda V \\
&= \arg \max_{u_\Omega} \left[\tilde{E}_\tau(u_\Omega, (u_i^k)_{i=1}^n) + \lambda \int_{\mathbb{R}} u_\Omega u_\Omega^k d\mathbf{x} \right]. \tag{26}
\end{aligned}$$

Notice that $\sum_{i=1}^n u_i^k = u_\Omega^k$. Thus (22) is an approximation of (26), and such an approximation becomes exact as $\tau' \rightarrow 0^+$.

To solve (22), similar to the first method, we relax the optimization to an equivalent problem: finding u_Ω^{k+1} such that

$$u_\Omega^{k+1} = \arg \max_{\substack{u_\Omega \in \mathcal{K} \\ \int u_\Omega = V}} \tilde{E}_{\tau, \tau'}^\lambda(u_\Omega, (u_i^k)_{i=1}^n), \tag{27}$$

where $\mathcal{K} := \{u \in BV(\Omega, \mathbb{R}) | u \in [0, 1]\}$. The proof of equivalence is similar to that of Lemma 3.1, and is omitted here.

The linearity of $\tilde{E}_{\tau, \tau'}^\lambda(u_\Omega, (u_i^k)_{i=1}^n)$ is computed as

$$L_{\tau, \tau'}^\lambda(u_\Omega, u_\Omega^k, (u_i^k)_{i=1}^n) = \int_{\mathbb{R}^d} u_\Omega \phi^k d\mathbf{x},$$

where the dominant function is

$$\phi^k(\mathbf{x}) = \sqrt{\frac{\pi}{\tau}} \left(S_{\tau/2}^k - \sum_{i=1}^n \left(G_{\tau/2} * u_i^k \right)^2 + (S_{\tau/2}^k)^{\frac{1}{2}} G_{\tau/2} * \left((S_{\tau/2}^k)^{\frac{1}{2}} (2u_\Omega^k - 1) \right) \right) + \lambda G_{\tau'} * \left(\sum_{i=1}^n u_i^k \right), \tag{28}$$

and $S_{\tau/2}^k$ denotes $S_{\tau/2}^k(\mathbf{x}) = G_{\tau/2} * \left(\sum_{i=1}^n u_i^k \right)(\mathbf{x})$. Then u_Ω^{k+1} can be computed by (18), the same as in the first method.

For the stopping criterion, the second method also uses β to control the update step-length, and reduces β when the rate of change of the averaged objective functional in a few iterations is less than the tolerance r_{tol} . The iteration stops when $\beta < \beta_{min}$, or when the total region between two consecutive steps are the same. The algorithm of the second method is summarized in Algorithm 4.

In the first method, the auction dynamics method is run several times in each iteration to find a partition, making the algorithm more stable and the partition more likely to be the global shortest

Algorithm 4: The second method for longest minimal length partitions

Input: Volume constraint V , partition proportions $\mathbf{c} = (c_1, \dots, c_n)$ satisfying $c_i > 0$ and $\sum_{i=1}^n c_i = 1$, time step $\tau > 0$, regularization parameter $\lambda > 0$, time step in regularization term $\tau' > 0$ auction dynamics parameters $\boldsymbol{\mu}$, update step-length parameters $0 \leq \beta_0 \leq 1, 0 < \gamma < 1, M \in \mathbb{N}, r_{tol} > 0, 0 < \beta_{min} < 1$

Output: u_Ω maximizing the objective functional, relative shortest partitions $(u_i)_{i=1}^n$

```

1 Set  $k = 0$ ; initialize  $u_\Omega^0$  randomly with  $\int u_\Omega^0 dx = V$ ;
2 Find  $(u_i^0)_{i=1}^n = ADM(u_\Omega^0, V, \mathbf{c}, \tau; \boldsymbol{\mu})$ ;
3 while  $\beta > \beta_{min}$  and not converge do
4   Compute dominant function  $\phi^k$  by (28) using  $\tau$  and  $\tau'$ ;
5   Update  $u_\Omega^{k+1}$  by (18);
6   Compute  $(u_i^{k+1})_{i=1}^n = ADM(u_\Omega^{k+1}, V, \mathbf{c}, \tau; \boldsymbol{\mu})$ ;
7   if  $k > M$  then
8     Compute  $E_{ave}^k = \frac{1}{M} \sum_{j=k-M+1}^k \tilde{E}_\tau(u_\Omega^j, (u_i^j)_{i=1}^n)$ ;
9     Compute  $E_{ave}^{k+1} = \frac{1}{M} \sum_{j=k-M+2}^{k+1} \tilde{E}_\tau(u_\Omega^j, (u_i^j)_{i=1}^n)$ ;
10    if  $|E_{ave}^{k+1} - E_{ave}^k| / |E_{ave}^{k+1}| < r_{tol}$  then
11       $\beta = \gamma\beta$ ;
12    end
13  end
14   $k = k + 1$ ;
15 end
16 Return  $u_\Omega = u_\Omega^k, (u_i)_{i=1}^n = (u_i^k)_{i=1}^n$ 

```

one instead of a local one. However, the computational complexity of this method is high. In the second method, a regularization term is added in the approximate objective functional for stability. It doesn't need to run the auction dynamics several times at every iteration in order to maintain the stability of the algorithm. Thus it is faster than the first method. Since the partition in each step may not be the global minimizer but a local one, the second method may need more iterations to converge.

4. Numerical experiments

We demonstrate the effectiveness of the proposed methods by experiments in two and three dimensions. Our methods are implemented by MATLAB. Convolutions are implemented using Fast Fourier Transform.

4.1. Numerical experiments in two dimensions

To simulate the longest minimal length partitions in two dimensions, a 256×256 regular grid is formed in $[-\pi, \pi]^2$ with a space step $\Delta x = 2\pi/256$. The time step is set to be $\tau = 2\Delta x \approx 0.049$, and $\tau' = 0.5\Delta x \approx 0.013$. The stopping parameters in the auction dynamics method are set to be $\boldsymbol{\mu} = (m, \epsilon_{min}, \alpha, \epsilon_0) = (1000, 10^{-7}, 4, 0.1)$. Other parameters are set as $\beta_0 = 1$ (the initial update rate for u_Ω), $\gamma = \frac{1}{2}$ (the decay factor of β), $\beta_{min} = 0,05$ (the lower bound of β), $M = 5$ (the number of steps in averaged objective functional) and $r_{tol} = 10^{-4}$. For the first method, auction dynamics repeat-time is $p = 5$. For the second method, regularization parameter is $\lambda = 10$.

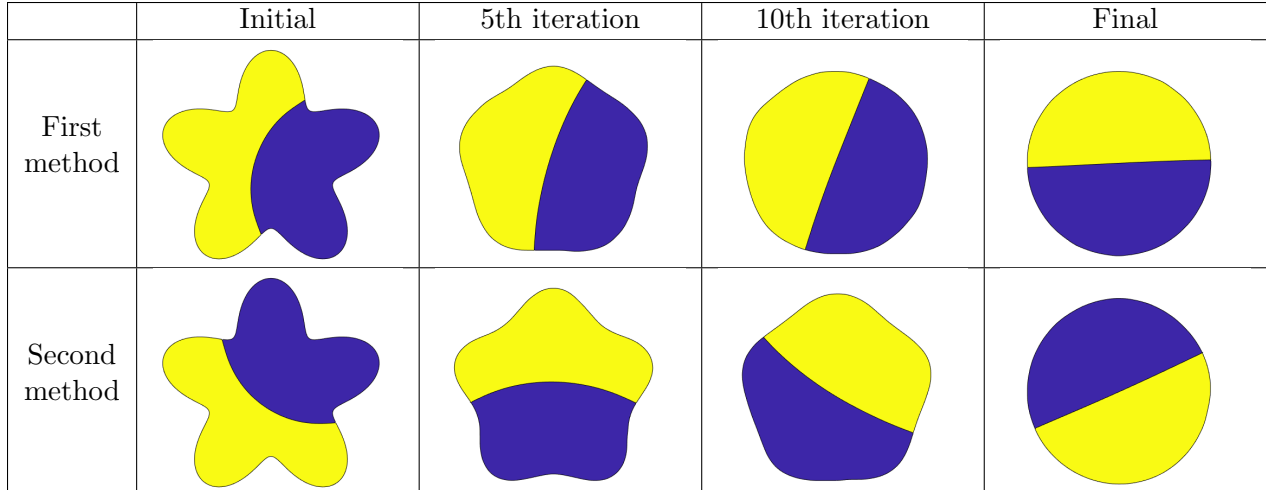


Figure 3: Two uniform partitions in two dimensions. The initial condition is set to be a five-petal flower. The total regions and their shortest partitions of both methods in the initial, 5th, 10th, and final iterations are plotted.

4.1.1. Two partitions

We first conduct experiments for the two dimensional example with two partitions of equal proportions. The initial condition is set to be a five-petal flower with the indicator function $\rho^2 < \pi^2(0.4 + 0.2 \sin 5\theta)$, where ρ and θ are the radius and angle in the polar coordinate respectively. The partition proportion is $\mathbf{c} = (\frac{1}{2}, \frac{1}{2})$. Both methods derived in Section 3 are implemented. The first method stops after 34 iterations, and the second method stops after 63 iterations. The total regions and their shortest partitions of both methods in the initial, 5th, 10th and final iterations are plotted in Figure 3. For visualization of the results, the indicator functions of the region and partitions are smoothed using a Gaussian kernel convolution before being plotted in Figure 3 and the figures in the following.

The evolution of the approximate objective functionals $\tilde{E}_\tau(u_\Omega^k, (u_i^k)_{i=1}^n)$ of both methods are plotted in Figure 4. As we can see, the final approximate objective functionals of two methods are both about 9.32. In the 10th iteration of the first method, the objective functional is near the final maximum objective functional, and the shape of total region shown in Figure 3 is close to a disc. Compared with the approximate objective functional of the second method, the approximate objective functional of first method has less fluctuation. This is because auction dynamics is repeated several times in each step of the first method, which increases the likelihood of obtaining a global shortest partition instead of a local minimizer. Thus the approximate objective functional in the first method should have a smaller gap with the exact objective functional compared to the second method.

To further confirm that we get a disc as the optimal total region, the isoperimetric inequality is checked for the final iteration results in Figure 3. For any simple-connected region Ω in 2d, we have

$$4\pi|\Omega| \leq |\partial\Omega|^2,$$

and the equality holds only when Ω is a disc. Using the indicator function of the initial condition, the area is computed to be $0.4\pi^3$. For the perimeter, we use the approximation

$$|\partial\Omega| \approx \sqrt{\frac{\pi}{\tau}} \int_{\mathbb{R}^d} u_\Omega G_\tau * (1 - u_\Omega) \mathrm{d}\mathbf{x}.$$

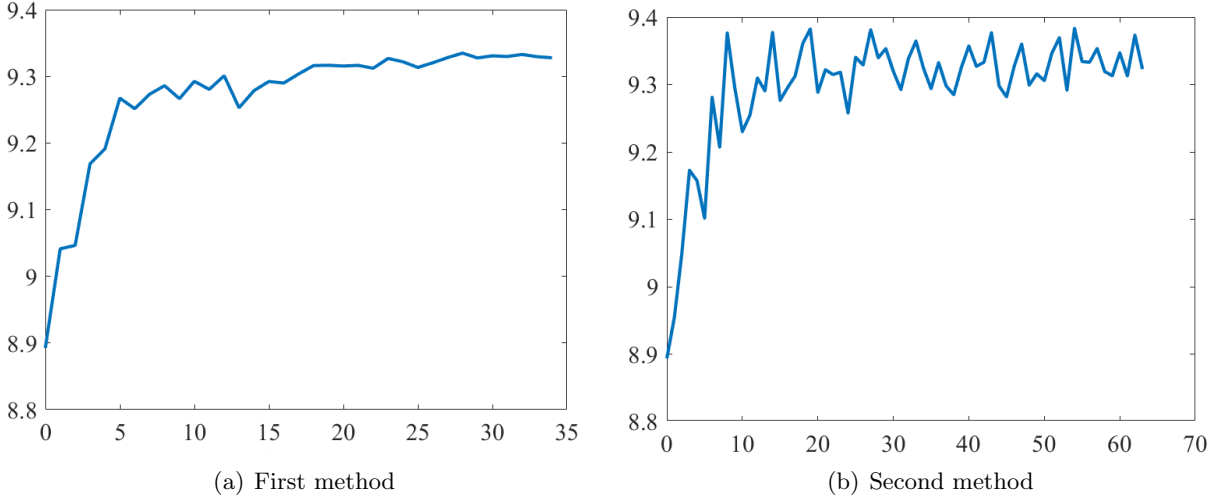


Figure 4: Two uniform partitions in two dimensions. The approximate objective functionals $\tilde{E}_\tau(u_\Omega^k, (u_i^k)_{i=1}^n)$ of two methods versus iteration times. The horizontal axis represents the number of iterations. The vertical axis represents the functional value.

Then the values of $4\pi|\Omega|/|\partial\Omega|^2$ for the results given by both methods are computed, which are 1.0056 and 1.0055. Here the final values are bigger than 1 due to the numerical error. Since they are close to 1, the isoperimetric inequality corroborates that the optimal total region by each method is a disc.

As the experiments show, for the uniform two-partition case, numerical simulations imply that the disc is the maximizer for longest minimal length partitions, which is compatible with the analytical results proved in [7].

4.1.2. Three partitions

We then test the proposed methods to find the optimal solution for three partitions with equal and unequal proportions. The volume proportion parameter \mathbf{c} is set to be $(\frac{1}{3}, \frac{1}{3}, \frac{1}{3})$, $(\frac{1}{4}, \frac{1}{4}, \frac{1}{2})$, $(\frac{1}{6}, \frac{1}{6}, \frac{2}{3})$, $(\frac{1}{6}, \frac{1}{3}, \frac{1}{2})$ and $(\frac{1}{10}, \frac{1}{5}, \frac{7}{10})$. The results of two methods are shown in Figure 5. As we can see, although the value of \mathbf{c} varies, the optimal total regions given by both methods keep to be a disc, and the partition results of both methods look similar.

4.1.3. Sensitivity to initial shape

We test the sensitivity of the proposed methods to the initial shape. In this experiment, both methods are used to find the optimal solution for three partitions with equal proportions. The shape of initial condition is set to be a triangle, a rectangle, and randomly generated pentagons. The results are shown in Figure 6. Both methods give the optimal total region to be a disc no matter how the shape of initial condition changes.

4.1.4. Six and nine partitions

In this set of experiments, the initial condition is set to be the five-petal flower, whose indicator function is given in Section 4.1.1. The two methods are tested to solve the six-partition and nine-partition problems. For each problem, the volume proportions of every part in the partitions are set to be equal. The total regions and their shortest partitions of both methods in the initial, 5th, 10th, 20th and final iterations are plotted in Figure 7.

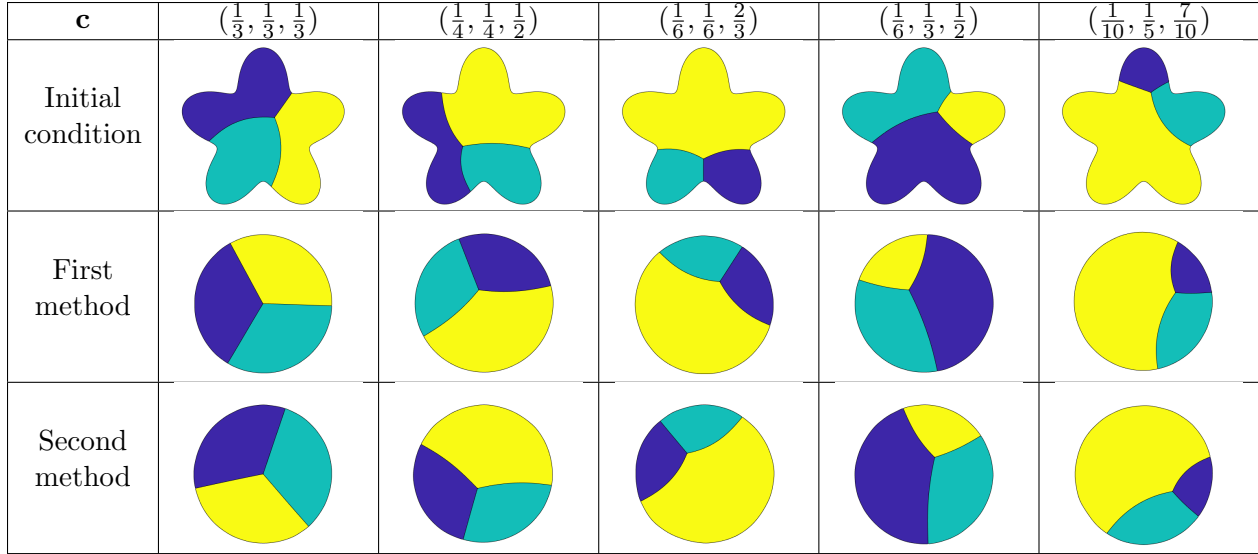


Figure 5: Three partitions in two dimensions. The initial condition is set to be a five-petal flower. The total regions and their shortest partitions of both methods in the final iterations are plotted for different values of \mathbf{c} of the three partition case.

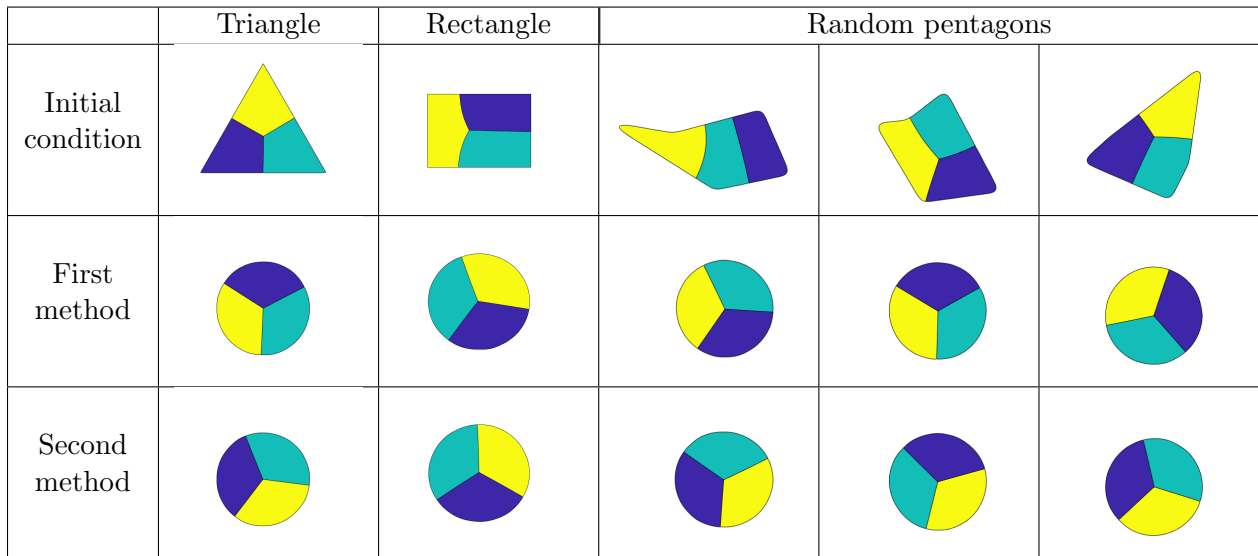


Figure 6: Three partitions in two dimensions, sensitivity to initial shape. The proportion is set to be $\mathbf{c} = (\frac{1}{3}, \frac{1}{3}, \frac{1}{3})$. The total regions and their shortest partitions of both methods in the final iterations are plotted for different shape of initial conditions.

The evolution of the approximate objective functional $\tilde{E}_\tau(u_\Omega^k, (u_i^k)_{i=1}^n)$ for both problems are plotted in Figure 8. We observe some irregular protrusions in the objective functional evolution. This is because the auction dynamics may give a local shortest partition instead of a global one in some iterations. Then the approximate objective functional is computed to be larger than the real objective functional, which leads to a protrusion. Since the first method repeats the auction dynamics several times, it is more likely to get a global shortest partition than the second method. Thus the first method has less protrusions on the objective functional evolution. This implies that the first method is more stable than the second one. However, since it repeats auction dynamics

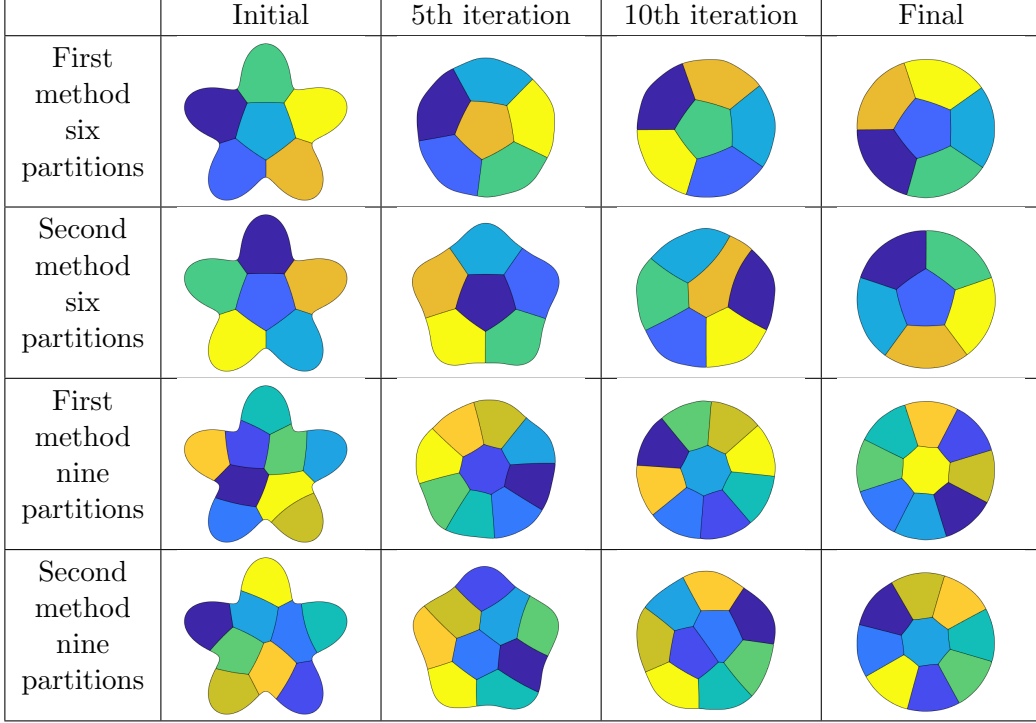


Figure 7: Six and nine uniform partitions in two dimensions. The initial condition is set to be a five-petal flower. The total regions and their shortest partitions of both methods in the initial, 5th, 10th, and final iterations are plotted.

No. of partitions	No. of Iter.		CPU time(s)	
	First method	Second method	First method	Second method
2	34	63	281.49	112.72
6	31	74	995.67	427.05
9	32	59	1611.79	650.43

Table 1: Uniform partitions in two dimensions. Number of iterations and CPU times of both methods with different numbers of partition.

many times, the first method requires more time than the second one in general. We show the CPU times of both methods with different numbers of partitions in Table 1. As mentioned above, even though the first method requires fewer iterations, since it repeats auction dynamics several times, its overall CPU time is higher than that of the second method.

4.2. Numerical experiments in three dimensions

To simulate the problem in three-dimensional cases, an $128 \times 128 \times 128$ regular grid is formed in $[-\pi, \pi]^3$. The tolerance of objective functional rate is set to be $r_{tol} = 0.0005$. For the first method, auction dynamics repeats $p = 3$ times in each iteration. Other parameters are the same as in two-dimensional cases. The initial total region is set to be a cube. We test both methods for three-partition, six-partition and nine-partition cases. The volume proportions of every part in the partitions are set to be equal in each case. The results of both methods are shown in Figure 9, together with an expanded view and a translucent expanded view.

In Figure 9, the solutions of the total region after convergence by the first method is consistent with the solutions of the second method. They both give a ball as the optimal solution for different

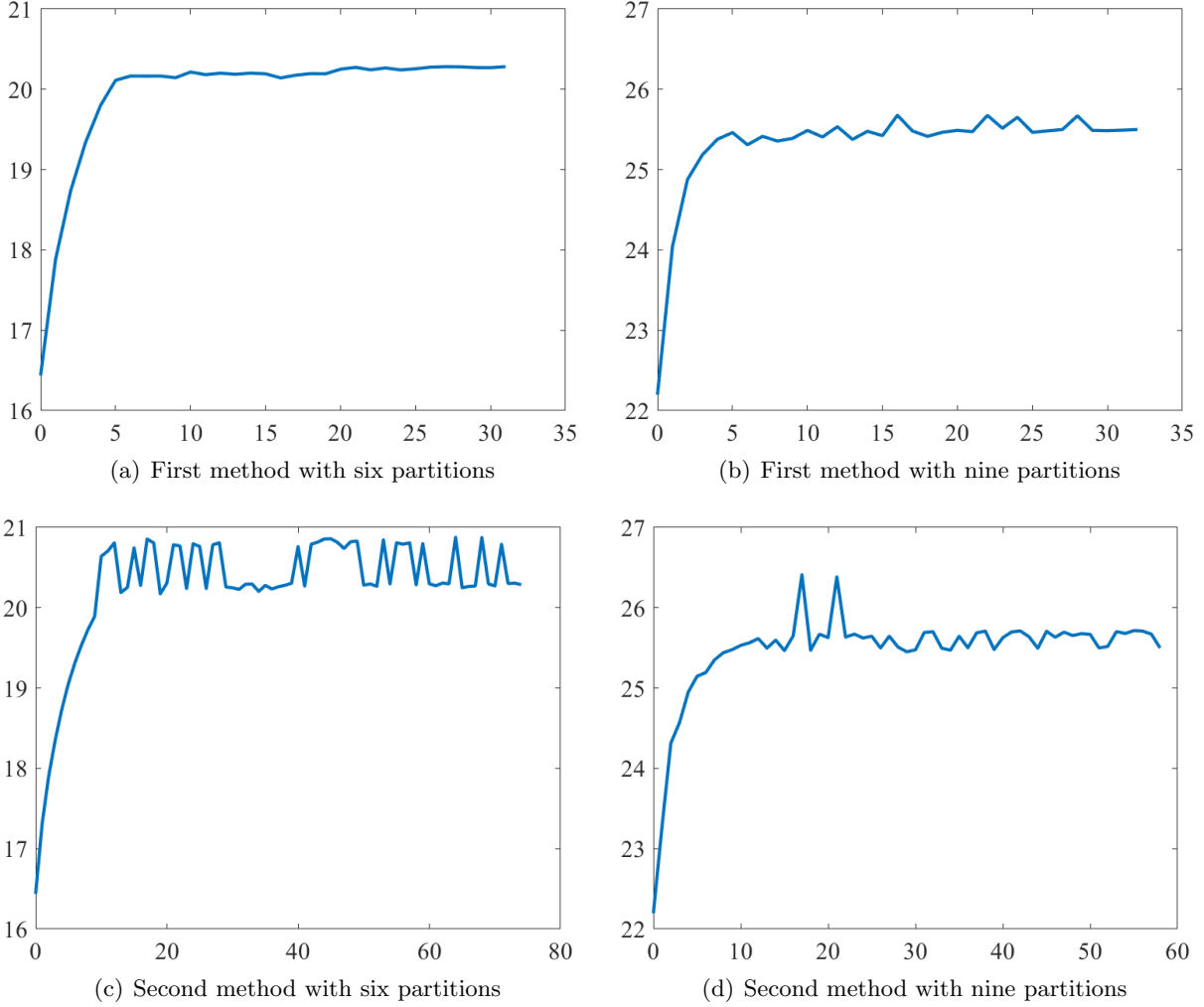


Figure 8: Six and nine uniform partitions in two dimensions. The approximate objective functionals $\tilde{E}_\tau(u_\Omega^k, (u_i^k)_{i=1}^n)$ of two methods versus iteration times. The horizontal axis represents the number of iterations. The vertical axis represents the functional value.

numbers of partitions. This numerically supports the conjecture that the ball is the maximizer of the longest minimal length partitions problem in three dimensions.

The evolution of approximate objective functionals for each experiment are shown in Figure 10. As the number of partitions increases, the approximate objective functional of final total region also increases. In each case, the objective functional by the first method is consistent to the objective functional by the second method.

The CPU time of both methods with different numbers of partitions are given in Table 2. Again, the second method uses more iterations but less GPU time compared to the first method.

5. An objective-functional-monotone method

Based on the first method, we further develop a method that promises the approximate objective functional is increasing during iterations. The idea is to check whether $\tilde{E}_\tau(u_\Omega^{k+1}, (u_i^{k+1})_{i=1}^n)$ is greater than or equal to $\tilde{E}_\tau(u_\Omega^k, (u_i^k)_{i=1}^n)$ in each step. If not, then $(u_i^k)_{i=1}^n$ is possible to be a

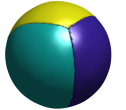
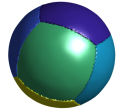
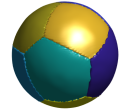
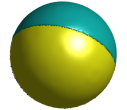
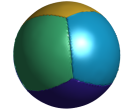
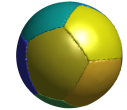
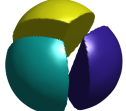
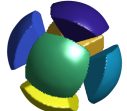
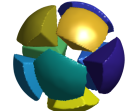

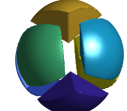
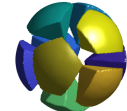


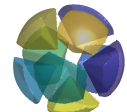
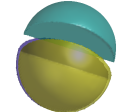
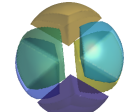
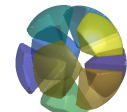
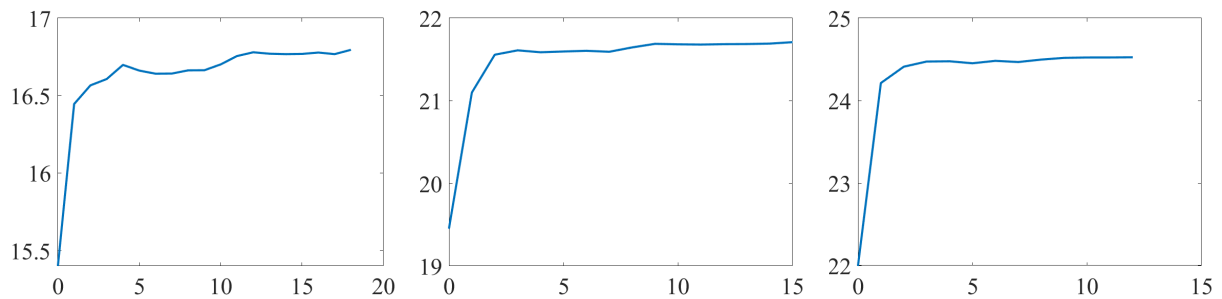
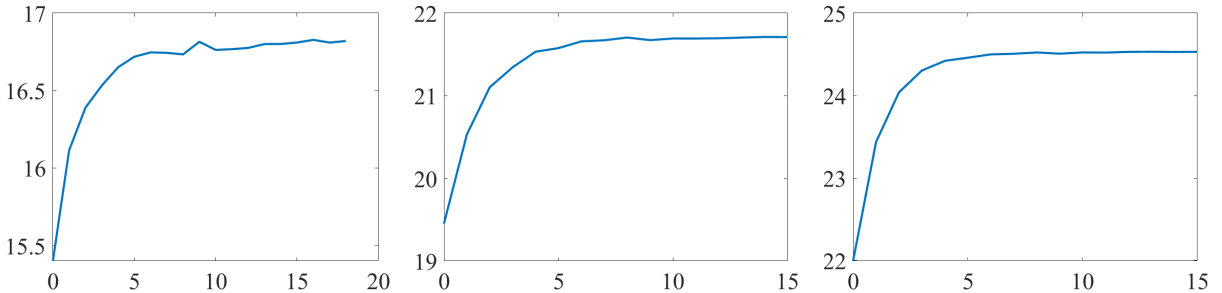
	First method			Second method		
Partition number	3	6	9	3	6	9
Final iteration						
An expanded view						
A translucent expanded view						

Figure 9: Uniform partitions in three dimensions. The initial condition is set to be a cube. The total regions and their shortest partitions of both methods in the final iteration (together with an expanded view and a translucent expanded view) are plotted for three-partition case, six-partition case and nine-partition case.



(a) First method with three partitions (b) First method with six partitions (c) First method with nine partitions



(d) Second method with three partitions (e) Second method with six partitions (f) Second method with nine partitions

Figure 10: Uniform partitions in three dimensions. The approximate objective functionals $\tilde{E}_\tau(u_\Omega^k, (u_i^k)_{i=1}^n)$ of the two methods versus iteration times. The horizontal axis represents the number of iterations. The vertical axis represents the functional value.

local minimizer instead of global shortest partition, or u_Ω^k is near the optimal solution. In this case, we just reduce β from 1, get new $u_\Omega^{k+1}, (u_i^{k+1})_{i=1}^n$, and check if the objective functional is increasing. If the objective functional is increasing, then the iterations keep going. Otherwise, β

No. of partitions	No. of Iter.		CPU time(s)	
	First method	Second method	First method	Second method
3	18	18	10678.05	2768.09
6	15	15	11053.22	4260.25
9	12	15	15129.92	6282.31

Table 2: Uniform partitions in three dimensions. Number of iterations and CPU times of both methods.













Iterations	2	4	6	8	10	12
Two-partition case						
Iterations	2	4	8	12	16	19
Three-partition case						

Figure 11: Objective-functional-monotone method. The initial condition is set to be a "five-petal flower". The total regions and their shortest partitions of the objective functional monotone method in some iterations are plotted for two-partition and three-partition cases with equal proportions.

is further reduced, and new $u_{\Omega}^{k+1}, (u_i^{k+1})_{i=1}^n$ are computed to compare the objective functional. If $u_{\Omega}^{k+1}, (u_i^{k+1})_{i=1}^n$ are not found to increase the objective functional, and β is reduced to 0, then $(u_i^k)_{i=1}^n$ is not a global shortest partition, or u_{Ω}^k is likely to be the optimal total region. To check which case it is, auction dynamics is repeated multiple times to find a partition of u_{Ω}^k with less objective functional than $(u_i^k)_{i=1}^n$. If such partition is found, then it is set to be the new $(u_i^k)_{i=1}^n$, and we take a step back to check whether $\bar{E}_{\tau}(u_{\Omega}^k, (u_i^k)_{i=1}^n)$ is greater than or equal to $\bar{E}_{\tau}(u_{\Omega}^{k-1}, (u_i^{k-1})_{i=1}^n)$. If such partition is not found, then we accept u_{Ω}^k to be the result, and $(u_i^k)_{i=1}^n$ is its shortest partition.

This method is tested for two-dimensional examples with two and three partitions and equal proportions. The total regions and their shortest partitions of both cases in some iterations are shown in Figure 11. The approximate objective functionals are shown in Figure 12. For two-partition case, this method uses 12 iterations and 3147.61 seconds. For three-partition case, this method uses 19 iterations and 3896.23 seconds. Although the method promises the objective functional is increasing, it spends ten times more CPU time than the first method for the two-partition case. This is because the new method uses a lot of time (many repetition of auction dynamics) for checking whether u_{Ω}^k and $(u_i^k)_{i=1}^n$ are global optimizers.

6. Conclusions

In this paper, two numerical methods are derived for the simulation of longest minimal length partitions problem. The methods are based on approximations of the objective functional by a short time heat flow, threshold dynamics, and splitting methods to solve the relative constrained max-min optimization problem. In both methods, auction dynamics is used to find the shortest partitions, and the update of total region is based on threshold dynamics. The shortest partitions and total region are updated in an alternative manner. To reduce the influence of local minimal partitions, the first method repeats auction dynamics several times in each iteration, and the second method introduces a proximal regularization term, which is shown to be equivalent to a gradient ascent flow. Both methods update the total region by introducing an update step-length,

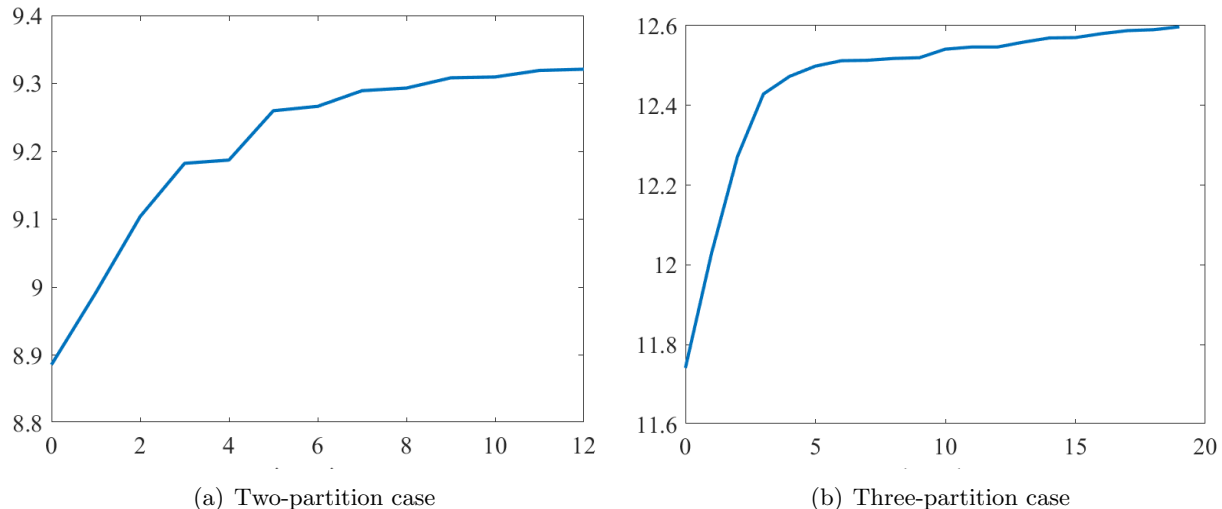


Figure 12: Objective-functional-monotone method for uniform partitions in two dimensions. The approximate objective functionals $\tilde{E}_\tau(u_\Omega^k, (u_i^k)_{i=1}^n)$ of both cases versus iteration times are plotted. The horizontal axis represents the number of iterations. The vertical axis represents the functional value.

which decreases gradually according to some criterion during iterations. The effectiveness of both methods are demonstrated by comprehensive numerical experiments, which validate the conjecture that the disc is the minimizer for two-dimensional problems and the ball is the minimizer for three-dimensional problems.

This paper focuses on the simulation to an approximate problem to provide the numerical evidence to the conjecture for the longest minimal length partitions problem. It would be interesting to consider the proof of the conjecture in the sense of the approximate objective functional and further consider the limit as τ goes to 0. It would be also interesting to use the level-set-based framework [41, 17, 42, 43] to approximate such problems.

Acknowledgements

H. Liu was partially supported by National Natural Science Foundation of China 12201530, HKRGC ECS 22302123, HKBU 179356. D. Wang was partially supported by National Natural Science Foundation of China (Grant No. 12101524), Guangdong Basic and Applied Basic Research Foundation (Grant No. 2023A1515012199) and Shenzhen Science and Technology Innovation Program (Grant No. JCYJ20220530143803007, RCYX20221008092843046), Hetao Shenzhen-Hong Kong Science and Technology Innovation Cooperation Zone Project (No.HZQSW-S-KCCYB-2024016) and the Guangdong Key Lab of Mathematical Foundations for Artificial Intelligence (2023B1212010001).

References

- [1] H. Auerbach, Sur un problème de M. Ulam concernant l'équilibre des corps flottants, *Studia Mathematica* 7 (1) (1938) 121–142.
- [2] K. Radziszewski, Sur les cordes qui partagent l'aire d'un ovale en 2 parties égales, *nakł. Uniwersytetu Marii Curie-Skłodowskiej*, 1956.

- [3] H. G. Eggleston, The maximal length of chords bisecting the area or perimeter length of plane convex sets, *Journal of the London Mathematical Society* 1 (1) (1961) 122–128.
- [4] P. Goodey, Area and perimeter bisectors of planar convex sets, in: *Integral Geometry And Convexity*, World Scientific, 2006, pp. 29–35.
- [5] G. Pólya, Aufgabe 283, *Elem. Math* 13 (1958) 40–41.
- [6] H. T. Croft, K. J. Falconer, R. K. Guy, *Unsolved problems in geometry*, Problem Books in Mathematics (1991).
- [7] L. Esposito, V. Ferone, B. Kawohl, C. Nitsch, C. Trombetti, The longest shortest fence and sharp Poincaré–Sobolev Inequalities, *Archive for Rational Mechanics and Analysis* 206 (3) (2012) 821–851.
- [8] W. Wichiramala, Efficient cut for a subset of prescribed area, *Thai J. Math.* 5 (3, Special issue) (2007) 95–100.
- [9] F. Morgan, Convex body isoperimetric conjecture, <https://sites.williams.edu/Morgan/2010/07/03/convex-body-isoperimetric-conjecture/> (2010).
- [10] J. Berry, E. Bongiovanni, W. Boyer, B. Brown, P. Gallagher, D. Hu, A. Loving, Z. Martin, M. Miller, B. Perpetua, S. Tammen, The convex body isoperimetric conjecture in the plane, *Rose-Hulman Undergraduate Mathematics Journal* 18 (2) (2017) 2.
- [11] B.-H. Wang, Y.-K. Wang, A note on the convex body isoperimetric conjecture in the plane, *Proceedings of the American Mathematical Society* 152 (02) (2024) 801–813.
- [12] B. Bogosel, E. Oudet, Longest minimal length partitions, *Interfaces and Free Boundaries* 24 (1) (2022) 95–135.
- [13] A. Braides, *Approximation of free-discontinuity problems*, no. 1694, Springer Science & Business Media, 1998.
- [14] M. Miranda Jr, D. Pallara, F. Paronetto, M. Preunkert, Short-time heat flow and functions of bounded variation in \mathbf{R}^N , in: *Annales de la Faculté des sciences de Toulouse: Mathématiques*, Vol. 16, 2007, pp. 125–145.
- [15] B. Merriman, J. K. Bence, S. Osher, *Diffusion generated motion by mean curvature*, Department of Mathematics, University of California, Los Angeles, 1992.
- [16] B. Merriman, J. Bence, S. Osher, *Diffusion generated motion by mean curvature*, AMS Selected Letters, Crystal Grower’s Workshop (1993) 73–83.
- [17] B. Merriman, J. K. Bence, S. Osher, Motion of multiple junctions: A level set approach, *Journal of Computational Physics* 112 (2) (1994) 334–363.
- [18] L. C. Evans, Convergence of an algorithm for mean curvature motion, *Indiana University Mathematics Journal* (1993) 533–557.
- [19] G. Barles, C. Georgelin, A simple proof of convergence for an approximation scheme for computing motions by mean curvature, *SIAM Journal on Numerical Analysis* 32 (2) (1995) 484–500.

- [20] S. Esedoglu, F. Otto, Threshold dynamics for networks with arbitrary surface tensions, *Communications on Pure and Applied Mathematics* 68 (5) (2015) 808–864.
- [21] S. J. Ruuth, B. Merriman, J. Xin, S. Osher, Diffusion-generated motion by mean curvature for filaments, *Journal of Nonlinear Science* 11 (2001) 473–493.
- [22] S. J. Ruuth, B. T. Wetton, A simple scheme for volume-preserving motion by mean curvature, *Journal of Scientific Computing* 19 (2003) 373–384.
- [23] M. Jacobs, E. Merkurjev, S. Esedoglu, Auction dynamics: a volume constrained MBO scheme, *Journal of Computational Physics* 354 (2018) 288–310.
- [24] S. Esedoglu, Y.-H. R. Tsai, Threshold dynamics for the piecewise constant Mumford–Shah functional, *Journal of Computational Physics* 211 (1) (2006) 367–384.
- [25] D. Wang, H. Li, X. Wei, X.-P. Wang, An efficient iterative thresholding method for image segmentation, *Journal of Computational Physics* 350 (2017) 657–667.
- [26] D. Wang, X.-P. Wang, The iterative convolution–thresholding method (ICTM) for image segmentation, *Pattern Recognition* 130 (2022) 108794.
- [27] X.-C. Tai, O. Christiansen, P. Lin, I. Skjælaaen, Image segmentation using some piecewise constant level set methods with MBO type of projection, *International Journal of Computer Vision* 73 (2007) 61–76.
- [28] X.-C. Tai, O. Christiansen, P. Lin, I. Skjælaaen, A remark on the MBO scheme and some piecewise constant level set methods, *UCLA CAM Rep* (2005) 05–24.
- [29] E. Merkurjev, T. Kostic, A. L. Bertozzi, An MBO scheme on graphs for classification and image processing, *SIAM Journal on Imaging Sciences* 6 (4) (2013) 1903–1930.
- [30] E. Merkurjev, E. Bae, A. L. Bertozzi, X.-C. Tai, Global binary optimization on graphs for classification of high-dimensional data, *Journal of Mathematical Imaging and Vision* 52 (2015) 414–435.
- [31] Z. M. Boyd, E. Bae, X.-C. Tai, A. L. Bertozzi, Simplified energy landscape for modularity using total variation, *SIAM Journal on Applied Mathematics* 78 (5) (2018) 2439–2464.
- [32] D. Wang, A. Cherkaev, B. Osting, Dynamics and stationary configurations of heterogeneous foams, *Plos one* 14 (4) (2019) e0215836.
- [33] M. Elsey, S. Esedoglu, P. Smereka, Diffusion generated motion for grain growth in two and three dimensions, *Journal of Computational Physics* 228 (21) (2009) 8015–8033.
- [34] X. Xu, D. Wang, X.-P. Wang, An efficient threshold dynamics method for wetting on rough surfaces, *Journal of Computational Physics* 330 (2017) 510–528.
- [35] H. Liu, J. Liu, R. Chan, X.-C. Tai, Double-well Net for image segmentation, *arXiv preprint arXiv:2401.00456* (2023).
- [36] H. Liu, X.-C. Tai, R. Chan, Connections between operator-splitting methods and deep neural networks with applications in image segmentation, *arXiv preprint arXiv:2307.09052* (2023).

- [37] X.-C. Tai, H. Liu, R. Chan, PottsMGNet: A mathematical explanation of encoder-decoder based neural networks, *SIAM Journal on Imaging Sciences* 17 (1) (2024) 540–594.
- [38] S. J. Ruuth, Efficient algorithms for diffusion-generated motion by mean curvature, *Journal of Computational Physics* 144 (2) (1998) 603–625.
- [39] K. Ishii, Optimal rate of convergence of the Bence–Merriman–Osher algorithm for motion by mean curvature, *SIAM Journal on Mathematical Analysis* 37 (3) (2005) 841–866.
- [40] D. Wang, An efficient iterative method for reconstructing surface from point clouds, *Journal of Scientific Computing* 87 (1) (2021) 38.
- [41] S. Osher, J. A. Sethian, Fronts propagating with curvature-dependent speed: Algorithms based on Hamilton-Jacobi formulations, *Journal of Computational Physics* 79 (1) (1988) 12–49.
- [42] T. F. Chan, X.-C. Tai, Level set and total variation regularization for elliptic inverse problems with discontinuous coefficients, *Journal of Computational Physics* 193 (1) (2004) 40–66.
- [43] J. Lie, M. Lysaker, X.-C. Tai, A piecewise constant level set framework, *Int. J. Numer. Anal. Model* 2 (4) (2005) 422–438.